

# New Insight into the Nature of Electron Delocalization: the Driving Forces for Distorting the Geometry of Stilbene-Like Species

Zhong-Heng Yu\* and Xiao-Qi Peng

State Key Laboratory for Structural Chemistry of Unstable & Stable Species, Institute of Chemistry, Chinese Academy of Sciences, Beijing 100080, People's Republic of China

Received: April 18, 2001; In Final Form: June 25, 2001

To understand the nature of electron delocalization while questioning the abnormally large torsional angle  $\theta$  of *N*-phenylmethylene-3-pyridineamine (**6**), we greatly improved our new program for energy partitioning. Meanwhile, the crystal structures of *N*-phenylmethylene-2-thiazoleamine (**1a**) and *N*-(4-nitro-phenyl)methylene-2-thiazoleamine (**1b**) were determined using X-ray diffraction. As shown by the optimized geometries of the molecules, such as **1a**, **1b**, (4-NO<sub>2</sub>-Ph)-CH=N-2-pyrimidyl, (4-NO<sub>2</sub>-Ph)-CH=N-2-pyridyl, and **6** with HF, DFT, MP2, and AM1, the results that  $d^2(E_e(\theta))/d|\theta|^2 > 0.0$  for total electronic energy and  $d^2(E_N(\theta))/d|\theta|^2 < 0.0$  for nuclear repulsion and  $d(E_e(\theta=42^\circ))/d|\theta|^2 = 0.0$  are not an artifact of a given optimized method, nor a distinct feature of a special molecule. As shown by the energy partitions, the  $\pi$ - $\pi$ ,  $\pi$ - $\sigma$ , and nonbonded  $\sigma$ - $\sigma$  interactions between fragments are always destabilization, and it is the nonbonded  $\sigma$ - $\sigma$  interaction, rather than the  $\pi$ - $\pi$  interaction, that distorts stilbene-like species away from their planar geometry. The destabilizing EX interactions between fragments is basically stabilization as far as its total effect on whole electronic state is considered. Correspondingly, the stabilizing CT interaction is practically destabilization. Thus, at the planar geometry, it is due to  $d(\text{CT})/d(r) < 0.0$ ,  $d(\text{EX})/d(r) < 0.0$ , or their sum  $d(\text{CT})/d(r) + d(\text{EX})/d(r) < 0.0$ , where  $r = r_{ab}$  or  $r_{14}$ , to shorten the length  $r_{14}$  of the bond C<sub>1</sub>-N<sub>4</sub> as well as to reduce the distance  $r_{ab}$  between fragments. A stilbene-like species has to distort itself away from its planar geometry in order to maintain its lowest total electronic energy  $E_e$  as far as possible when the attractive force  $d(E_e(\theta))/d(r_{ab}) > 0.0$  is not large enough to balance the resistance force  $d(V_{ab})/d(r_{ab}) < 0.0$ . Resistances to the distortion arise from the destabilizing  $\pi$ - $\sigma$  interaction and from the  $dE_N(\theta)/d|\theta| > 0.0$ . At a geometry with about  $\theta = 52^\circ$ ,  $d(\Delta E(\theta))/d|\theta| = 0$  is a compromise between the nonbonded  $\sigma$ - $\sigma$  and  $\pi$ - $\sigma$  interactions, and it is approximately in accord with the  $d(E_e(\theta=42^\circ))/d|\theta| = 0.0$  obtained from standard Gaussian 98 program.

## 1. Introduction

One of the most important cornerstones in the framework of the organic chemical thought is the knowledge that a molecule with conjugated double bonds has a higher thermodynamic stability than those of isomeric compounds having isolated double bonds. The standard textbook explanation for this stability is given in terms of resonance stabilization.<sup>1</sup> It is also one of the fundamental concepts that the maximum resonance energy results from the planarity of  $\pi$  system.<sup>1,2</sup> However, the abnormally large torsional angle of stilbene-like species seems to challenge the viewpoint of resonance stabilization.<sup>3a</sup>

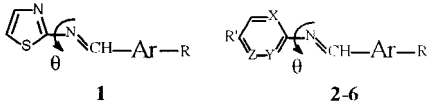
The marked dissimilarity in the electronic spectra of stilbene and *N*-benzylideneaniline (NBA) has led to a great number of theoretical and experimental studies and arguments in the past three decades.<sup>4</sup> The resonance stabilization is always used to interpret the effects of substituents on the conformations of stilbene-like species.<sup>5</sup> Burgi and recent researchers ascribed the large torsional angle to the repulsive interaction between the hydrogen on the -N=CH- and one of the ortho hydrogens on the aniline ring.<sup>6</sup> The loss of the  $\pi$  electron energy in the torsional geometry can be compensated for partly by the charge transfer (CT-2) from the bridge nitrogen lone pair to the phenyl ring and by the decrease in steric hindrance.<sup>6a</sup> These researchers expected, therefore, that if the nonbonded interaction was neglected, the  $\pi$  electron transfer between the conjugated fragments would be found to favor the planar conformation of

NBA.<sup>7</sup> Burgi's conclusion appears to be questioned by the angles  $\theta$  (both up to 30°) of stilbene and azobenzene in gas state.<sup>8</sup>

To discern whether conjugation effect depends on conformation or results in a nonplanar geometry and to compare the effects of various aromatic rings, such as five- and six-membered and condensed rings, on the geometry, we prepared the following 9 compounds: (4-X-Ph)-CH=N-2-thiazolyl (**1a**, X = H; **1b**, X = NO<sub>2</sub>), (4-NO<sub>2</sub>-Ph)-CH=N-2-pyrimidyl (**2**), (4-NO<sub>2</sub>-Ph)-CH=N-2-pyridyl (**3**), Ph-CH=N-1-naphthyl (**4**), and (4-X-Ph)<sub>2</sub>C=C=N-(Ph-Y-4) (**5a**, X = H, Y = H; **5b**, X = H, Y = NO<sub>2</sub>; **5c**, X = MeO, Y = NO<sub>2</sub>; **5d**, X = H, Y = N(Me)<sub>2</sub>); and we determined their crystal structures using X-ray diffraction. The crystal structures of molecules **2**, **3**, and **5** have been published elsewhere,<sup>3a</sup> and the crystallographic data of **5** were used to argue against the viewpoint that the large torsional angle ( $\theta = 41^\circ$ ) of (4-N(Me)<sub>2</sub>-Ph)-CH=N-(Ph-NO<sub>2</sub>-4) is due to the CT-2 interaction.<sup>9</sup> As for the nonbonded contact, molecules **2** and **3** should be comparable to **1** and **5**, but the experimental angles  $\theta$  (20–26°) for the former are generally larger than those (0–16°) for the latter (Table 1).

When 22 rotational geometries of each of five molecules **1a**, **1b**, **2**, **3**, and **6** (Ph-CH=N-3-pyridyl<sup>10</sup>) are optimized with B3lyp/6-311G\*\* and the differences  $\Delta E_e(\theta) = E_e(\theta) - E_e(0^\circ)$  in total electronic energy and  $\Delta E_N(\theta)$  in total nuclear repulsion are plotted as the functions of the angle  $\theta$  in Figure 1, we would argue that a driving force for distorting the molecule away from

\* Corresponding author. FAX: 86-10-62559373. E-mail: yuzh@infoc3.icas.ac.cn.

TABLE 1: Experimental and Theoretical Values (deg) of the Torsional Angle  $\theta$  in Stilbene-like Species


compounds	Ar	X	Y	Z	R	R'	AMI	RHF/6-311G**	B3lyp/6-311G**	X-ray
<b>1a</b>	Ph				H	H	90°	37°	0°	9°
<b>1b</b>	Ph				NO <sub>2</sub>	H	90°	37°	0°	4°
<b>2</b>	Ph	N	N	CH	NO <sub>2</sub>	H	50°	—	22°	26°
<b>3</b>	Ph	CH	N	CH	NO <sub>2</sub>	H	0°	—	0°	20°
<b>4<sup>a</sup></b>	Ph	CH	CH	CH	H	H			47°	53°
<b>6</b>	Ph	CH	CH	N	H	H	38°	—	42°	46°

<sup>a</sup> The thiazolyl group in **1a** has been replaced with naphthenyl group.

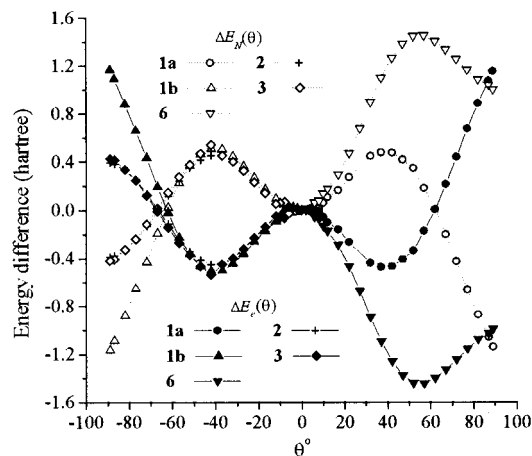


**Figure 1.** Differences  $\Delta E_c(\theta) = E_c(\theta) - E_c(0^\circ)$  and  $\Delta E_n(\theta)$  in total electronic energy and nuclear repulsion and their changes with the torsional angle  $\theta$ . The geometries were optimized with B3lyp/6-311G\*\*.

its planar geometry arises from the electron interaction rather than from nuclear repulsion. Molecules **2** and **6** exist preferentially in a “crowded” geometry<sup>11</sup> with  $\theta > 20^\circ$  (Figure 1 and Table 1).

In our previous work,<sup>3,12</sup> we developed a new program for calculating vertical resonance energy according to the principle of the Morokuma’s energy partition,<sup>13</sup> and we argued that in the case of stilbene-like species, the  $\pi$  electron delocalization is always destabilization and it prefers a distorted geometry rather than a planar geometry. But the detail energy partitions implied that the  $\pi$ - $\pi$  interaction should not be a main driving force. Besides, Figure 1 also means that there should be another force to resist the distortion. To search for the unknown driving forces as well as to understand the nature of electron delocalization arising from the  $\pi$ - $\pi$ ,  $\pi$ - $\sigma$ , and  $\sigma$ - $\sigma$  interactions, our new procedure, i.e., Morokuma’s energy partitioning based on the fragment molecular orbital (FMO) basis set, is greatly improved in this work. On the basis of the Morokuma’s energy partition, the energy effect, associated with a specific electron interaction between fragments, is partitioned into its exchange (EX) and charge transfer (CT) components. The roles of the EX and CT interactions in causing electron delocalization and in determining the molecular behavior are distinguished and evaluated, and the sensitivities of the geometric data to the EX and CT interactions are compared by means of four Gaussian basis sets within the RHF functional. In addition, various atomic interaction energies are calculated with the standard Gaussian procedure, and their effects on the bond length and bond angle are investigated with the aim of supporting the conclusions derived from Morokuma’s energy partitioning analysis.

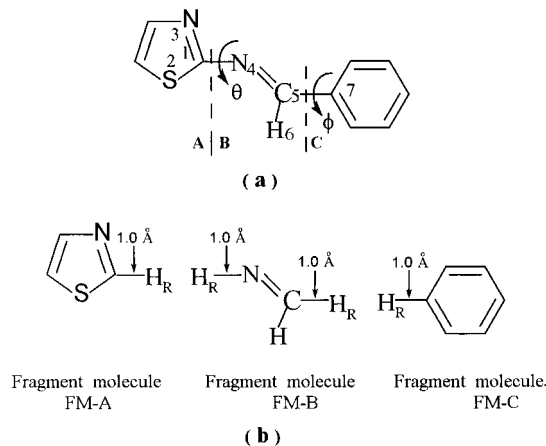


**Figure 2.** (a) Dissection way and numbering system in *N*-phenylmethene-2-thiazoleamine (**1a**). The A–B–C dissection of **1a** into a phenyl fragment (A), an imine group (B), and a 2-thiazolyl fragment (C). (b) Formation of the corresponding fragment molecules denoted as FM-A, FM-B, and FM-C.

## 2. Methods

According to the PMO (perturbation molecular orbital) theory,<sup>11,14</sup> we can consider a nonplanar molecule **1a**, for example, as three planar opened-shell fragments, a phenyl fragment (A), an imine group –CH=N– (B), and a 2-thiazolyl fragment (C), i.e., A–B–C dissection as shown in Figure 2. Generally, the dissection way depends on the number of the planar fragments in a specific molecule. Accordingly, molecule **1b** should be dissected into four fragments, and the fourth one is a nitro group (D).

The FMO basis set  $\{\psi_i, \psi_j, \psi_l\}$  for molecule **1a**, for example, is obtained from the superposition of three sub-FMO basis sets. Each sub-basis consists of the doubly occupied, vacant, and singly occupied FMOs. In the FMO basis set, each FMO has correct electron occupancy and is absolutely localized on its corresponding fragment. In particular, the  $\pi$  and  $\sigma$  systems in each sub-basis have been separated out thoroughly. The FMO basis can be expressed as the following:

$$\psi_i = \sum_{k=1}^{N_a} a_{ki} \phi_k + \sum_{m=N_a+1}^{N_a+N_b} a_{mi} \phi_m + \sum_{n=N_a+N_b+1}^N a_{ni} \phi_n \quad (1)$$

$$\psi_j = \sum_{k=1}^{N_a} a_{kj} \phi_k + \sum_{m=N_a+1}^{N_a+N_b} a_{mj} \phi_m + \sum_{n=N_a+N_b+1}^N a_{nj} \phi_n \quad (2)$$

$$\psi_l = \sum_{k=1}^{N_a} a_{kl} \phi_k + \sum_{m=N_a+1}^{N_a+N_b} a_{ml} \phi_m + \sum_{n=N_a+N_b+1}^N a_{nl} \phi_n \quad (3)$$

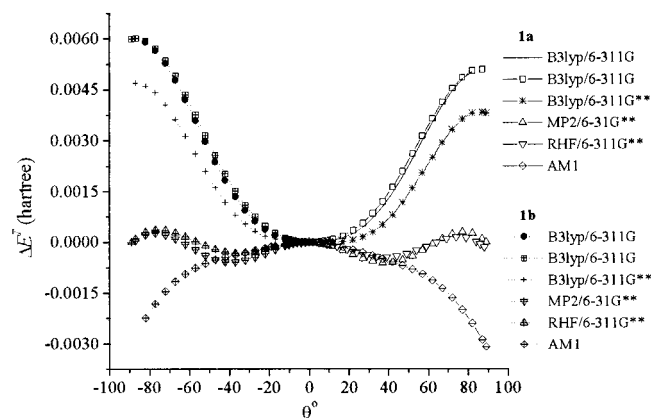


**Figure 3.** Differences  $\Delta E^T(\theta) = E^T(\theta) - E^T(0^\circ)$  in molecular energy  $E^T(\theta)$  and their changes with the optimized methods as well as with the torsional angle  $\theta$ . (A solid line without the central symbol and a dotted line with the central solid cycles were obtained from the full optimization for molecules **1a** and **1b** at B3lyp/6-311G level).

where the atomic orbitals (AOs)  $\phi_k$  ( $k=1, 2, \dots, N_a$ )  $\in$  fragment A,  $\phi_m$  ( $m=N_a+1, \dots, N_a+N_b$ )  $\in$  B, and  $\phi_n$  ( $n=N_a+N_b+1, \dots, N$ )  $\in$  C,  $a_{ki}$ ,  $a_{mi}$ ,  $a_{ni}$ , etc., are their coefficients, and all  $a_{mi}$  and  $a_{ni}$ ,  $a_{kj}$  and  $a_{nj}$ , and  $a_{kl}$  and  $a_{ml}$  are set equal to zero;  $N_a$ ,  $N_b$ , and  $N$  are the numbers of AOs in fragments A and B and the whole molecule, respectively. The construction of the FMO basis set  $\{\psi_i, \psi_j, \psi_l\}$  is a four-step procedure, and it has been detailed elsewhere.<sup>3,12</sup> The FMO basis set can also be expressed as  $\{\psi^{\sigma_m}, \psi^{\sigma_n}\}$ , where  $m, n \in$  the whole molecule. Occasionally, it is expressed as  $\{\psi^{\sigma_m}, \psi^{\sigma_n}, \psi^{\sigma_k}\}$ , where  $n \in$  doubly occupied and vacant  $\sigma$  FMOs and  $k \in$  singly occupied  $\sigma$  FMOs,  $k \neq n$ .

### 3. Results and Discussion

**3.1. Geometry Optimization.** The rotational geometries of each of the stilbene-like species were optimized with the HF (Hartree–Fock), MP2 (second-order Møller–Plesset perturbation), DFT (density functional theory), and AM1 methods in the Gaussian 98 program, respectively. The starting geometry of each molecular conformation was taken from its crystal structure. The conformational space was sampled by varying  $\theta$  in steps of  $2^\circ$  for  $0^\circ < \theta < 12^\circ$  and steps of  $5^\circ$  for  $12^\circ < \theta < 90^\circ$ . To simplify the procedure for separating out the  $\pi$  and  $\sigma$  systems thoroughly, at each point, we carried out the geometry optimization under the following conditions: each aromatic ring, including its hydrogen atoms, was kept coplanar; the angle  $\theta$  was kept constant during the period of the optimization. With the purpose of proving that the energies  $E_c(\theta)$  and  $E_N(\theta)$  calculated at the constrained geometries are reasonable as far as their first- and second-order derivatives,  $d(E_c(\theta))/d\theta$  and  $d^2(E_c(\theta))/d\theta^2$ , are concerned, we selected **1a** and **1b** as two representative molecules and fully optimized their geometries at B3lyp/6-311G level, with the exception that the angle  $\theta$  was still kept constant at each point (a solid line without the central symbol and a dot line with the central solid cycles in Figures 3 and 4).

As shown by the curves in Figure 3 and the data in Table 1, the preferential geometry of molecule **1a**, for example, depends on the optimized methods, and  $d(E_c(\theta))/d\theta = 0.0$  at  $\theta = 90^\circ$  (AM1),  $37^\circ$  (RHF/6-311G\*\* and MP2/6-31G\*\*), and  $0^\circ$  (B3lyp/6-311G and 6-311G\*\*). According to our calculations of the vertical resonance energy, the aromatic behavior of a five-membered ring is very different from that of a six-membered ring.<sup>3b</sup> However, all curves in Figure 4, together with those in Figure 1, show identically  $d^2(\Delta E_c(\theta))/d\theta^2 > 0.0$  and  $d^2(\Delta E_N(\theta))/$

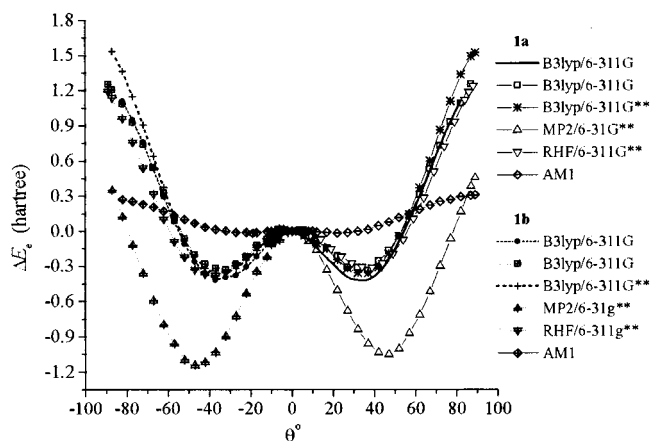


**Figure 4.** Differences  $\Delta E_c(\theta) = E_c(\theta) - E_c(0^\circ)$  in total electronic energy  $E_c(\theta)$  and their changes with the optimized methods as well as the torsional angle  $\theta$ . (A solid line without central symbol and a dashed line with the central solid cycles were obtained from the full optimization for **1a** and **1b** at B3lyp/6-311G).

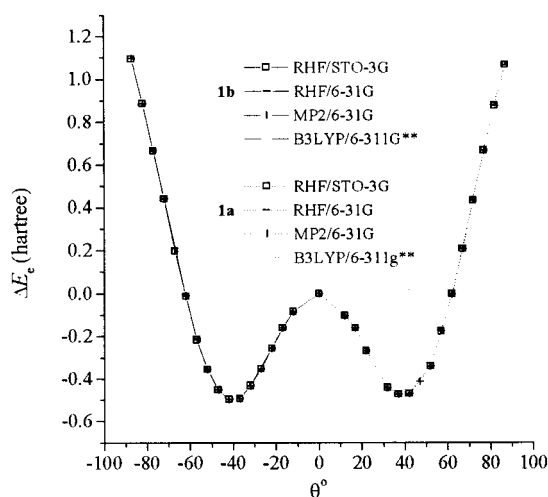
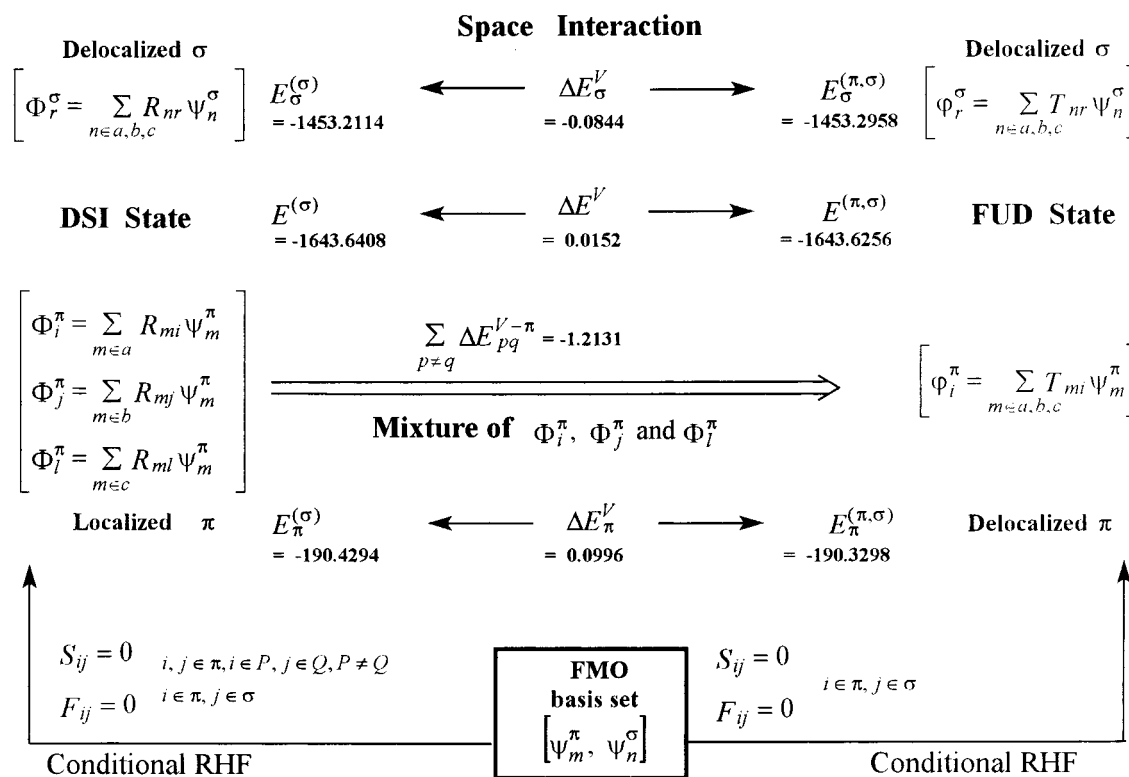


**Figure 5.** Total electronic energy differences  $\Delta E_c(\theta) = E_c(\theta) - E_c(0^\circ)$  obtained from HF, MP2, and DFT computations for the same series of the geometries (B3lyp/6-311G\*\*) and their changes with the angle  $\theta$ .

$d|\theta|^2 < 0.0$ . Particularly,  $d(\Delta E_c(\theta))/d|\theta| = 0.0$  at about  $\theta = 42^\circ$  is almost not an artifact of a given optimized method, nor a distinct feature of a specific molecule. In the hypothetical vibrationless state, the preferential geometry of a molecule is sure to be a compromise between  $d(\Delta E_c(\theta))/d|\theta| = d(E_c(\theta))/d|\theta| < 0.0$  and  $d(\Delta E_N(\theta))/d|\theta| = d(E_N(\theta))/d|\theta| > 0.0$ . In the region of the torsional angle from 0 to  $\pm 40^\circ$ , as shown by an inspection of Figures 1 and 3, the difference between  $|d(E_c(\theta))/d\theta|$  and  $d(E_N(\theta))/d\theta$  is so small that the torsional angle of stilbene-like species in the solid state possibly will be sensitive to packing force and it may perhaps be sensitive to shrinkage in the gas phase.

In this work, the FMO basis set and various orbital interaction energies are constructed and calculated at the STO-3G level for the optimized geometry with B3lyp/6-311G\*\* if there is no special indication (the phrase, such as “the optimized geometry with B3lyp/6-311G\*\*”, is often shortened to “the geometry (B3lyp/6-311G\*\*)” hereafter). The molecular geometries, including its fragments and fragment molecules, are no longer optimized during the period of the energy partitions. We have presented several reasons why RHF/STO-3G is more reasonable for the Morokuma’s energy partition elsewhere.<sup>3b</sup> Figure 5 may provide it with one more deduction. In this figure, four curves

## SCHEME 1



were obtained from the regular computations with HF, MP2, and DFT for the same series of the rotational geometries (B3lyp/6-311G\*\*), and they fully overlap each other. It seems that the electron correction has, as expected by Kollmar,<sup>15</sup> a slight influence on the energy effects arising from electron delocalization. In fact, it was also emphasized in the literature<sup>6b</sup> that the geometric parameters of stilbene are more sensitive to the exchange functional rather than the correlation functional.

**3.2.  $\pi$  Electron Delocalization Is Destabilization.** Scheme 1 is a thermodynamic cycle for the orbital interactions in a geometry with  $\theta = 0^\circ$  (B3lyp/6-311G\*\*) of molecule **1a**. It shows the symbols for various  $\pi$  and  $\sigma$  electronic energies in the following two fictitious electronic states: the **DSI** state  $\{\Phi_r^\sigma, \Phi_i^\pi, \Phi_j^\pi, \Phi_l^\pi\}$  with a delocalized  $\sigma$  framework  $\{\Phi_r^\sigma; r \in A, B, C\}$  and three localized  $\pi$  systems  $\{\Phi_i^\pi, \Phi_j^\pi, \Phi_l^\pi; i \in A, j \in B, l \in C\}$ ; the fully delocalized state  $\{\varphi_r^\sigma, \varphi_i^\pi; r, i \in A, B, C\}$  denoted as **FUD**. At a planar geometry, the **FUD** is the ground state. The energy differences  $\Delta E_\pi^V$  and  $\Delta E_\sigma^V$  between these two states can be expressed as the following formulas:

$$\Delta E_\pi^V = E_\pi^{(\pi,\sigma)} - E_\pi^{(\sigma)} = \left( \sum_{q < p}^{\text{all}} E_{pq}^{(\pi,\sigma)-\pi} \right) + \sum_p^{\text{all}} (E_p^{(\pi,\sigma)-\pi} - E_p^{(\sigma)-\pi}) \quad (4)$$

$$\Delta E_\sigma^V = E_\sigma^{(\pi,\sigma)} - E_\sigma^{(\sigma)} \quad (5)$$

where  $p, q =$  fragments A, B, C and the symbol  $E_p^{(\pi,\sigma)-\pi}$  denotes the  $\pi$  energy of fragment P in the FUD state. In the right side of eq 4,  $\Delta E_{pq}^{V-\pi}$  is an energy effect associated with the  $\pi$  interaction (local resonance interaction) between fragments P and Q, and  $\Delta E_p^{V-\pi}$  measures the effect of the local resonance interaction on the original  $\pi$  system of fragment P. The energy effect  $\Delta E_\sigma^V$  is the response of whole  $\sigma$  framework to the

delocalization of the  $\pi$  electrons, and it arises from the influence of the  $\pi$  electron delocalization on the  $\sigma$ - $\pi$  space interactions expressed in terms of the Coulomb  $J_{\sigma\pi}$  and exchange  $K_{\sigma\pi}$  integrals.<sup>3</sup> The sum  $\Delta E_\pi^V + \Delta E_\sigma^V$  is the so-called vertical resonance energy  $\Delta E^V$ .<sup>15,16</sup> In the Morokuma's energy partition, the components  $E_{pq}^{(\pi,\sigma)-\lambda}$  and  $E_p^{(\pi,\sigma)-\lambda}$  ( $\lambda = \pi, \sigma$ ) of total electronic energy in the FUD state, for example, are obtained from the following general expression:

$$E_{pq}^{(\pi,\sigma)-\lambda} = \sum_{ij} (F_{ij}^{(\pi,\sigma)-\lambda} + H_{ij}^{(\pi,\sigma)-\lambda}) D_{ij}^{(\pi,\sigma)-\lambda} \quad i \in P, j \in Q; P \neq Q \text{ or } P = Q \quad (6)$$

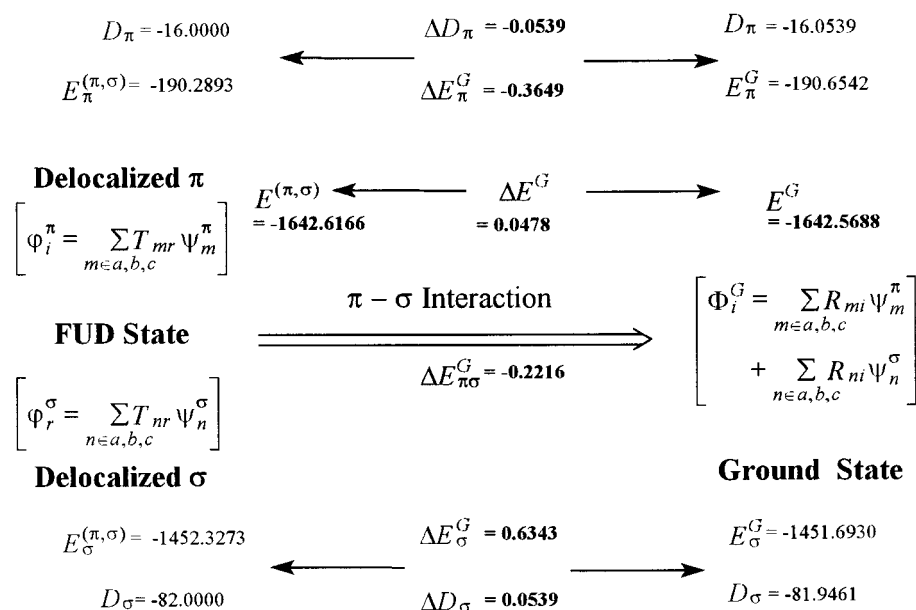
where **F**, **H**, and **D** are Fock, Hamiltonian, and density matrixes, respectively (a capital bold letter denotes a matrix over the FMO basis);  $F_{ij}^{(\pi,\sigma)-\lambda}$ ,  $H_{ij}^{(\pi,\sigma)-\lambda}$ , and  $D_{ij}^{(\pi,\sigma)-\lambda}$  are their respective elements that are obtained from the RHF (restricted Hartree-Fock) computations, over the FMO basis set, for a specific geometry under the conditions presented in Scheme 1.

Similar to the conclusion in our previous work,<sup>3a</sup>  $\Delta E^V$  in Table 2 is always destabilization. The practical calculations show furthermore that  $\Delta E^V$  is also destabilizing when the optimization of a planar geometry and the Morokuma's energy partition are performed at the same Gaussian basis set. Thus,  $\Delta E^V(\theta) > 0.0$  and  $d(\Delta E^V(\theta))/d|\theta| < 0.0$  are the basic features of the  $\pi$ -delocalization although the size of the Gaussian basis set has a great influence on the value of  $\Delta E^V$ .<sup>15,17</sup>

In this work, we will pay great attention to the ways that the delocalization of electrons influences the  $\pi$  (or  $\sigma$ ) system itself and the  $\sigma$  ( $\pi$ ) framework as well as affects the behaviors of electron donor and acceptor. For this reason,  $\Sigma \Delta E_{pq}^{V-\pi}$  is partitioned into  $\Sigma \Delta E_{pq}^2$  and  $\Sigma \Delta E_{pq}^4$ . Here,  $\Sigma \Delta E_{pq}^4$  is the EX energy effect associated with the four-electron interactions between fragments P and Q, and  $\Sigma \Delta E_{pq}^2$  arises from CT, which mixes the occupied FMO of fragment P with the vacant FMO



## SCHEME 2



of fragment Q and vice versa. At the geometry with  $\theta = 0^\circ$  (B3lyp/6-311G\*\*) of **1a**, for example, the CT energy effect ( $-1.92037$  hartrees) predominates over the EX one ( $0.77856$  hartrees) at the STO-3G level, and the ratio  $R_{XC} = \text{EX}/|\text{CT}|$  for the same geometry increases as the Gaussian basis becomes larger. Correspondingly,  $\Sigma \Delta E_{pq}^{V-\pi}$  ( $-1.21313$  hartrees) and  $\Delta E_{\sigma}^V$  ( $-0.08444$  hartrees) are most stabilizing at the STO-3G level, and they ( $0.33736$  and  $0.15162$  hartrees) become most destabilizing at the 6-31G level. Meanwhile,  $\Delta E_{\pi}^V$  is getting more stabilizing as the Gaussian basis set increases.

It seems that the EX is overestimated at the higher Gaussian basis level according to the following detailed partitions for the geometry with  $\theta = 0^\circ$  (B3lyp/6-311G\*\*) of **1a**: at the 6-31G level, some of two electron interaction energies  $\Delta E_{ij}^2$  are destabilizing, and their values are, for example,  $0.24821$  hartrees when  $i = 17$  and  $j = 91$ th FMOs,  $0.13059$  hartree when  $i = 21$  and  $j = 91$ th FMOs, and  $0.33747$  hartree when  $i = 27$  and  $j = 66$ th FMOs ( $i, j \in \pi$ ). These energy effects are not in agreement with the fundamental concepts of the PMO theory.<sup>11,18</sup> But such examples have never been found at the STO-3G level.

**3.3.  $\pi$ - $\sigma$  Interaction Is Destabilization.** Owing to the high order perturbation,<sup>19</sup> it is impossible to define a fictitious electronic state in which all orbital interactions were, artificially, excluded except for the  $\pi$ - $\sigma$  interaction between fragments P and Q. Thermodynamically, the ground state  $\{\Phi_i^G\}$  in Scheme 2 can also be considered as an electronic state resulted from the interaction between the  $\pi$   $\{\varphi_i^{\pi}\}$  and  $\sigma$   $\{\varphi_r^{\sigma}\}$  systems in the FUD state. In Scheme 2,  $\Delta E_{\pi\sigma}^G$  ( $-0.2216$  hartrees) is the energy effect associated with the interaction between the  $\pi$  and  $\sigma$  systems in the geometry with  $\theta = 87^\circ$  (B3lyp/6-311G\*\*) of molecule **1a**, and  $\Delta E_{\sigma}^G$  ( $0.6343$  hartrees) and  $\Delta E_{\pi}^G$  ( $-0.3649$  hartrees) measure the effects of the interaction on the  $\sigma$  and  $\pi$  systems themselves.

The eigenvectors of the FUD and the ground states are, respectively, obtained from the conditional (Scheme 1) and the full RHF computations, over the same FMOs basis set  $\{\psi_m^{\pi}, \psi_n^{\sigma}\}$ , for the same rotational geometry, and they can be expressed as the linear combination, as shown by  $\{\varphi_i^{\pi}, \varphi_r^{\sigma}\}$  and  $\{\Phi_i^G\}$  in Scheme 2, of the FMOs as well as the linear combination of atomic orbitals (AOs). Thus, it is easy to

**TABLE 2:  $\pi$  Interaction Energy  $\Sigma \Delta E_{pq}^{V-\pi}$  between Fragments P and Q and Its CT and EX Components, the Vertical Resonance Energy  $\Delta E^V$  and Its Two Components  $\Delta E_{\pi}^V$  and  $\Delta E_{\sigma}^V$  in Each of Four Typical Rotational Geometries (B3LYP/6-311G\*\*) of **1a**, and Their Changes with the Gaussian Basis Set (Energy Unit in hartrees)**

$\theta$ (deg)	$\Sigma \Delta E_{pq}^{V-\pi}$	$\Sigma \Delta E_{pq}^2$ (CT)	$\Sigma \Delta E_{pq}^4$ (EX)	$\Delta E_{\pi}^V$	$\Delta E_{\sigma}^V$	$\Delta E^V$ (VRE)
RHF/STO-3G						
0	-1.21313	-1.92037	0.77856	0.09961	-0.08444	0.01517
12	-1.17996	-1.87315	0.76178	0.09614	-0.08132	0.01483
42	-0.86746	-1.42132	0.59336	0.05982	-0.04834	0.01148
89	-0.47052	-0.82329	0.34485	-0.00129	0.00817	0.00687
RHF/3-21G						
0	-0.23203	-1.81018	1.63764	0.00000	0.06213	0.06214
12	-0.19046	-1.75274	1.60198	-0.00322	0.06395	0.06073
42	0.04936	-1.22526	1.29677	-0.03791	0.08405	0.04614
89	-0.12167	-0.83968	0.69099	0.12249	-0.09925	0.02324
RHF/4-31G						
0	0.00543	-1.59401	1.63970	-0.04012	0.10462	0.06450
12	0.05699	-1.51903	1.63950	-0.04293	0.10587	0.06294
42	0.26963	-1.00561	1.30926	-0.06937	0.11618	0.04682
89	-0.26260	-0.91054	0.61201	-0.10833	0.12870	0.02038
RHF/6-31G						
0	0.33736	-1.38119	1.75146	-0.08233	0.15162	0.06929
12	0.39296	-1.30391	1.72887	-0.08385	0.15146	0.06761
42	0.57288	-0.81527	1.38903	-0.09856	0.14874	0.05018
89	-0.18592	-0.86183	0.63867	-0.12576	0.14765	0.02189

calculate the population  $Q_i$  on each of the FMOs and then to get total  $\pi$  and  $\sigma$  electron charges  $D_{\lambda} = \Sigma Q_i$  ( $i \in \lambda$ ;  $\lambda = \pi, \sigma$ ) in each of these two electronic states using the well-known method.<sup>20</sup> When  $\Delta E_{\lambda}^2 = \Delta E_{\text{ov}}^{\rho\lambda} - \Delta E_{\text{ov}}^{\lambda\rho}$  is defined as the CT energy difference arising from the transferring of the net charge  $\Delta D_{\lambda} < 0.0$  from the  $\rho$  system to the  $\lambda$  one,  $\Delta D_{\lambda}$  is the linear function of  $\Delta E_{\lambda}^2$ . As shown by Figure 6,  $|\Delta D_{\lambda}|$  increases while  $|\Delta E_{\lambda}^2|$  is getting larger as the torsional angle  $|\theta|$  increases. Here,  $\Delta E_{\text{ov}}^{\rho\lambda}$  is the CT energy effect associated with the mixture of the occupied FMOs of the  $\rho$  system and the vacant FMOs of the  $\lambda$  system. In addition,  $\Delta D_{\lambda}$  and  $\Delta E_{\lambda}^2$  can also be considered as the net electron charge and CT energy gain of the  $\lambda$  system. When  $\Delta E_{\lambda} = \Delta E_{\lambda}^G$  ( $\lambda = \pi, \sigma$ ), it is, as revealed by Figure 7, the linear function of  $\Delta D_{\lambda}$ . Accordingly, the  $\pi$  system is always an electron acceptor ( $\Delta D_{\pi} < 0.0$  and  $\Delta E_{\pi}^2 < 0.0$ ), and it is stabilized, i.e.,  $\Delta E_{\pi}^G < 0.0$ . On the other hand, the  $\sigma$  system, as an electron-releasing system ( $\Delta D_{\sigma} = |\Delta D_{\pi}| > 0.0$  and  $\Delta E_{\sigma}^2 =$

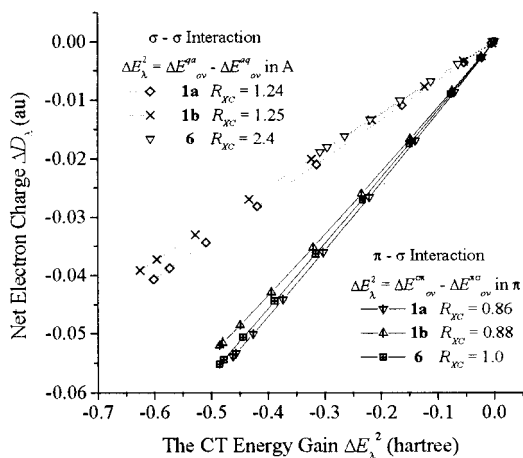


**Figure 6.** Linear relationship between the net electron charge and the CT energy gain of the  $\lambda$  system at STO-3G level, where the symbol  $\pi$  denotes the  $\pi$  system in the  $\pi$ - $\sigma$  interaction, and the symbol A the  $\sigma$  system of fragment A in the  $\sigma$ - $\sigma$  nonbonded interaction.

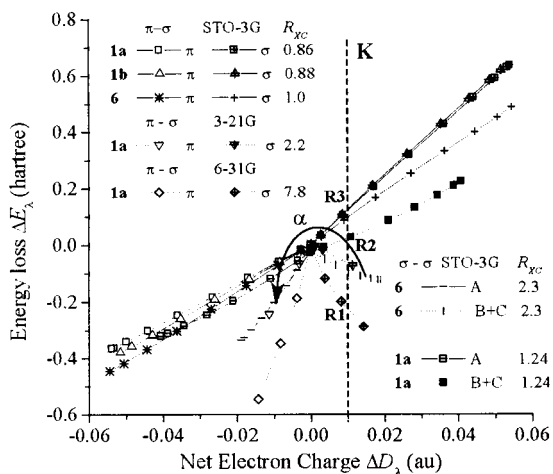


**Figure 7.** Energy loss (or gain)  $\Delta E_\lambda$  of the  $\lambda$  system is, approximately, the linear function of its net electron charge  $\Delta D_\lambda$ , and  $d(\Delta E_\lambda)/d(\Delta D_\lambda)$  changes with  $R_{XC}$ , where the symbol  $\pi$  denotes  $\Delta E_\lambda = \Delta E_\pi^G$  and  $\sigma$  denotes  $\Delta E_\lambda = \Delta E_\sigma^G$  in the  $\pi$ - $\sigma$  interaction and the symbol A denotes  $\Delta E_\lambda = \Delta E_a^{(\sigma)-\sigma}$  and B + C denotes  $\Delta E_\lambda = \Delta E_{b+c}^{(\sigma)-\sigma}$  in the  $\sigma$ - $\sigma$  interaction.

$|\Delta E_\pi^2| > 0.0$ ), is always destabilized, i.e.,  $\Delta E_\sigma^G > 0.0$ , and  $\Delta E_\sigma^G > |\Delta E_\pi^G|$ . As a result, total energy effect, as shown by  $\Delta E^G = \Delta E_{\pi\sigma}^G + \Delta E_\pi^G + \Delta E_\sigma^G$  in Table 3 and Scheme 2, is always destabilizing at the STO-3G level, and  $d(\Delta E^G(\theta))/d|\theta| > 0.0$ .

### 3.4. Nonbonded $\sigma$ Interaction is a Main Driving Force.

**3.4.1. Nonbonded  $\sigma$  Interaction between Fragments.** We have indicated that the  $\sigma$ -delocalization is destabilization in hexagonal  $H_6$ .<sup>3b</sup> But it is difficult to do so when the dissection of a molecule, as shown by Figure 2, involves the breaking of the  $\sigma$  bonds. In this case, all inter- and intrafragment elements  $F_{ij}$  and  $S_{ij}$  ( $i, j \in \sigma$  and  $i$  or  $j$ , not both,  $\in$  singly occupied FMOs) in the reference state with localized  $\sigma$  electrons have to be set equal to zero in order to prevent the high order perturbation besides the interfragment elements  $F_{ij} = 0.0$  and  $S_{ij} = 0.0$  ( $i, j \in \sigma$  and  $i, j \notin$  singly occupied FMOs).<sup>3,12a</sup> Nevertheless, it is feasible to comprehend the role of the interactions between the nonbonded  $\sigma$  FMOs first. For this reason, two more electronic states, denoted as DSI'  $\{\Phi_r^\sigma, \Phi_S, \Phi_i^\pi, \Phi_j^\pi, \Phi_l^\pi\}$  and FUL  $\{\varphi_r^\sigma, \varphi_t^\sigma, \varphi_s, \varphi_i^\pi, \varphi_j^\pi, \varphi_l^\pi\}$  in Scheme 3, should be characterized. According to the conditions for RHF computations, there is a delocalized  $\sigma$  system II, as described by  $\{\varphi_S\}$  and  $\{\Phi_S\}$  respectively in

Scheme 3, in each of the two electronic states, and it results from the linear combination of all singly occupied localized FMOs  $\psi_k^S$ . In the case of **1a**, the number of the singly occupied FMOs is four, and the total electron charge of the system  $\{\Phi_S\}$  is about  $-3.9$  au. The electronic occupations of the FUL and DSI' states are correct. The two delocalized  $\sigma$  systems  $\{\Phi_S\}$  and  $\{\Phi_r^\sigma\}$  in the DSI' state are independent of each other. Thus, the DSI' can also be considered as an electronic state arising from the interaction, i.e., the nonbonded  $\sigma$ - $\sigma$  interaction, between two localized  $\sigma$  systems  $\{\varphi_r^\sigma; r \in A\}$  and  $\{\varphi_t^\sigma; t \in B + C\}$  in the FUL state.

The energy effect  $\Sigma \Delta E_{aq}^{(\sigma)-\sigma}$ , associated with the nonbonded  $\sigma$  interactions between fragments A and Q ( $Q = B, C$ ), is a sum of CT, EX, and  $\Delta E_{vv}^{aq}$  (Table 4). Here,  $\Delta E_{vv}^{aq}$  arises from the interaction between the vacant  $\sigma$  FMOs, and it is so small that it does not be concerned in this work. In Scheme 3, the difference in total electronic energy between the DSI' and FUL states is  $\Delta E^{(\sigma)} = E^{(\sigma)} - E^L = \Delta E_\pi^{(\sigma)} + \Delta E_\sigma^{(\sigma)} = (\Sigma \Delta E_p^{(\sigma)-\pi}) + (\Sigma \Delta E_r^{(\sigma)-\sigma} + \Sigma \Delta E_{aq}^{(\sigma)-\sigma})$ , where  $p = A, B, C, r = A, B + C$ , and  $q = B, C$ . As shown by the data in Table 4,  $\Delta E^{(\sigma)}$  is always destabilizing, and  $d(\Delta E^{(\sigma)}(\theta))/d|\theta| < 0$ . However, it is not enough yet to say that the nonbonded  $\sigma$  interaction is destabilization just due to  $\Sigma \Delta E_{aq}^{(\sigma)-\sigma} > 0.0$ .

**3.4.2. Exchange and CT Interactions.** Electron delocalization is an important concept in modern organic chemistry. There is no single definition underlying use of this concept throughout chemistry.<sup>21</sup> As shown by comparison of the data such as  $\Delta E_\sigma^G$  in Table 3 and  $\Sigma \Delta E_r^{(\sigma)-\sigma}$  in Table 4, the nonbonded  $\sigma$ - $\sigma$  interaction at RHF/STO-3G level is different from the  $\pi$ - $\sigma$  interaction at same basis level, but it is similar to the latter at the larger Gaussian basis level. On the basis of Morokuma's definition,<sup>13</sup> the roles of the EX and CT interactions in causing electron delocalization should be detailed.

As an electron-withdrawing system, the net electron charge  $\Delta D_\lambda$  ( $\lambda = \sigma$ ) of the  $\sigma$  system of the fragment A is also the linear function of its CT energy gain  $\Delta E_\lambda^2 = \Delta E_{ov}^{aq} - \Delta E_{ov}^{aq}$  ( $\lambda = \sigma$  and  $q = B + C$ ) in the nonbonded  $\sigma$ - $\sigma$  interaction (Figure 6), and its  $|\Delta D_\lambda|$  is decreasing while its  $|\Delta E_\lambda^2|$  is getting smaller as the angle  $|\theta|$  increases. Particularly,  $R_{XC}$  has a slight effect on  $d(\Delta D_\lambda)/d(\Delta E_\lambda^2)$  of the functional lines in Figure 6 as far as a specific type of the electron interaction is concerned. It appears that  $\Delta E_\lambda^2$  determines the degree of electron delocalization. Here,  $R_{XC}$  for the  $\pi$ - $\sigma$  interaction is the ratio EX/|CT| in the geometry with  $\theta = 87^\circ$  (B3lyp/6-311G\*\*), and that for the  $\sigma$ - $\sigma$  interaction refers to the ratio in the geometry with  $\theta = 0^\circ$ .

In Figure 7, the functional lines are plotted in pairs. Each pair corresponds to a specific electron interaction and describes quantitatively the effects of  $\Delta D_\lambda$  on the donor and acceptor themselves while the fragment A rotates about the bond  $C_1-N_4$ . Similar to the  $\pi$ - $\sigma$  interaction, an electron-withdrawing system itself ( $\Delta D_\lambda < 0.0$ ,  $\lambda = \sigma$ ), such as the  $\sigma$  system of fragment A, is always stabilized, i.e.,  $\Delta E_\lambda = \Delta E_a^{(\sigma)-\sigma} < 0.0$  in Figure 7. Whether the electron-releasing system itself, such as the  $\sigma$  system in the  $\pi$ - $\sigma$  interaction and the  $\sigma$  system of fragment B + C in the nonbonded  $\sigma$ - $\sigma$  interaction, is stabilized or not depends on the value of  $R_{XC}$ . When  $R_{XC}$  is about 0.86–1.25, it is destabilized, i.e.,  $\Delta E_\lambda = \Delta E_{b+c}^{(\sigma)-\sigma} > 0.0$  and  $\Delta E_\lambda = \Delta E_\sigma^G > 0.0$ . However, the obtuse angle  $\alpha$  between a pair of the functional lines is getting larger as the value of  $R_{XC}$  increases, no matter which type of the orbital interaction is involved. Particularly,  $R_{XC}$  has much greater effect on  $d(\Delta E_\lambda)/d(\Delta D_\lambda)$  of the functional line for an electron-releasing system. When  $R_{XC}$



**TABLE 4: Various Energy Effects Arising from the  $\sigma$ - $\sigma$  Nonbonded Interaction between Fragments A and B + C at the STO-3G Level and the Net  $\sigma$  Electron Charge  $\Delta D_\sigma$  (atomic units) in the  $\sigma$  System of Fragment A<sup>a</sup>**

$\theta$ (deg)	$\Sigma\Delta E_{aq}^{(\sigma)-\sigma}$	$\Sigma\Delta E_{aq}^2$ (CT)	$\Sigma\Delta E_{aq}^4$ (EX)	$\Delta D_\sigma$	$\Sigma\Delta E_p^{(\sigma)-\pi}$	$\Sigma\Delta E_r^{(\sigma)-\sigma}$	$\Delta E^{(\sigma)}$
				<b>1a</b>			
0	0.16493	-0.71587	0.88109	-0.04067	-0.02691	-0.09687	0.05733
12	0.16853	-0.68078	0.84974	-0.03874	-0.02563	-0.10234	0.05595
42	0.15955	-0.36543	0.52589	-0.02105	-0.01437	-0.11218	0.04130
87	0.07055	-0.01063	0.08120	-0.00025	-0.00123	-0.04892	0.02061
				<b>1b</b>			
0	0.18631	-0.74651	0.93282	-0.03914	-0.02807	-0.11788	0.05758
-12	0.18877	-0.70953	0.89846	-0.03726	-0.02675	-0.12226	0.05613
-42	0.17586	-0.37817	0.55483	-0.02010	-0.01483	-0.12852	0.04128
-87	0.07165	-0.01098	0.08266	-0.00022	-0.00123	-0.05042	0.02021
				<b>6</b>			
0	0.55325	-0.42461	0.97737	-0.01889	-0.03417	-0.45682	0.06860
12	0.54074	-0.40528	0.94564	-0.01808	-0.03284	-0.44707	0.06690
42	0.35743	-0.22112	0.57885	-0.01009	-0.01998	-0.29391	0.04706
87	0.06525	-0.00856	0.07383	-0.00004	-0.00152	-0.04429	0.01968

<sup>a</sup>  $p = a, b, c$ ;  $r = a, b + c$ .  $q = b, c$ .

concerned, the CT interaction appears to be basically destabilization although the corresponding CT energy effects such as  $\Sigma\Delta E_{pq}^2$  (Table 2),  $\Delta E_{ov}^{\pi\sigma} + \Delta E_{ov}^{\sigma\pi}$  (Table 3), and  $\Sigma\Delta E_{aq}^2$  (Table 4), in themselves, are stabilizing. The EX interaction is an attempt to stabilize the whole electronic state as far as possible in such a way that  $d(\Sigma\Delta E_{aq}^{(\sigma)-\sigma})/d(\text{EX}) > 0$  and  $d(\Delta E_r^{(\sigma)-\sigma})/d(\text{EX}) < 0$ . Only when it is further realized that the forces,  $d(\text{EX})/d(r_{ab}) < 0$ ,  $d(\text{CT})/d(r_{ab}) < 0$  or the sum  $(d(\text{EX})/d(r_{ab}) + d(\text{CT})/d(r_{ab})) < 0$ , are practically attractive, where  $r_{ab}$  is the average distance between fragments A and B, can we argue that the nonbonded  $\sigma$ - $\sigma$  interaction is destabilization.

Before doing so, it is necessary to describe briefly the interaction, denoted as I-II, between two  $\sigma$  systems  $\{\Phi_r^\sigma\}$  and  $\{\Phi_S\}$  in the DSI' state first. The DSI in Scheme 1 can also be considered as an electronic state resulted from the I-II interaction. In the geometry with  $\theta = 0^\circ$  (B3lyp/6-311G\*\*) of **1a**, for example, the local energy effect  $\Delta E_{\text{I,II}}$  associated with the I-II interaction is  $-2.0079$  hartrees. One of its components, arising from this interaction between fragments A and Q ( $Q \neq A$ ), is  $-0.36406$  hartrees, the contribution to  $\Delta E_{\text{I,II}}$  made by all intra-fragment interactions is  $-1.40351$  hartrees, and the remainder ( $-0.24033$  hartrees) results from the interaction between fragments B and C. But it is still an insoluble mystery whether the I-II interaction between fragments A and Q is stabilization or not although the I-II interaction strongly stabilizes whole electronic state by  $\Delta E = -0.70711$  hartrees. In addition,  $d(\Delta E^{(\sigma)}(\theta))/d|\theta| < 0.0$  in the nonbonded  $\sigma$ - $\sigma$  interaction, and also  $d(\Delta E(\theta))/d|\theta| < 0.0$  in the I-II interaction, but  $|d(\Delta E^{(\sigma)}(\theta))/d\theta|$  is about 2 times greater than  $|d(\Delta E(\theta))/d\theta|$  according to our practical calculations. Therefore, it is reasonable to expect that the contribution to  $|d(\Delta E(\theta))/d\theta|$ , only made by the I-II interaction between fragment A and Q, should be much smaller than that to  $|d(\Delta E^{(\sigma)}(\theta))/d\theta|$ . The I-II interaction between fragments A and Q should have a slight effect on the torsional angle  $\theta$ , and it is not important in this work as far as the driving forces are concerned.

**3.4.3. Local Destabilizing Interaction between Fragments Is Practically Attractive.** Theoretically, we may specify a electronic state obtained from the conditional RHF computation in which all interfragment  $F_{ij}$  and  $S_{ij}$ , except for those between the occupied  $\sigma$  FMOs, are set equal to zero in order to examine the role of the EX interaction in the  $\sigma$  electron delocalization. But the problem is that this electronic state may violate Pauli exclusion principle.<sup>22</sup> As we have known, the size of the Gaussian basis set has a great effect on the EX interaction. In

literature,<sup>6b</sup> it was also found that all predicted bond lengths of stilbene, it was also found that all predicted bond lengths of stilbene are somewhat reduced as the size of the Gaussian basis set is increased from 3-21G to 6-31G. For these reasons, the coplanar geometries ( $\theta = 0^\circ$ ,  $\phi = 0^\circ$ ) of each of molecules **1a**, **2b**, **3b**, and **6** were optimized with the RHF/STO-3G, 3-21G, 4-31G, and 6-31G, respectively, and their geometric data are presented in Figure 8. Various orbital interaction energies in Table 5 were obtained from the Morokuma's energy partition at the same Gaussian basis level as the geometry was optimized. To support the conclusions derived from our program for energy partitioning, we obtained various atomic interaction energies, together with their  $\pi$  and  $\sigma$  components, from the standard Gaussian program for calculating total electronic energy. In Table 6,  $A_{m,n}$  is the atomic energy effect associated with the interaction between the  $m$  and  $n$ th atoms in the ground state,  $A_{a,n}$  refers to the energy effect arising from the interaction between the whole fragment A and the  $n$ th atom in fragment B, and  $A_{ab}$  is a sum of all nonbonded atomic interaction energies between fragments A and B. As shown by data in Table 5 and 6, the difference in any energy effect between two optimized geometries of a specific molecule predominates over that in its corresponding  $\pi$  component. It is reasonable that various energy effects, rather than their  $\sigma$  components, will be used in the following discussion for convenience.

At the optimized geometry (STO-3G) of molecule **1a**, for example, the energy effects, such as  $\Sigma\Delta E_{aq}$  ( $-5.80593$  hartrees),  $A_{a,4}$  ( $-7.13154$  hartrees), and  $A_{1,4}$  ( $-8.10377$  hartrees), are most stabilizing, and the ratio of  $\Sigma\Delta E_{aq}$  to total electronic energy  $E_c$  is the largest of the four geometries (STO-3G to 6-31G). Interestingly, the length  $r_{14}$  ( $1.446 \text{ \AA}$ ) of the bond  $C_1-N_4$  is the longest rather than the shortest (Figure 8). On the other side, the ratio  $R_{\text{XC}}$  ( $0.088$ ) is the smallest in the geometry (STO-3G) and increases from  $0.58$  (3-21G) to  $1.06$  (6-31G) despite the facts that  $\Sigma\Delta E_{aq}^2$  ( $-8.07465$  hartrees) is most stabilizing in the geometry (3-21G) and those ( $-8.07465$  and  $-6.35696$  hartrees) in the geometries (3-21G and 4-31G) are more stabilizing than in the geometry (STO-3G). Correspondingly, the nuclear repulsion energy  $V_{ab}$  ( $108.21061$  hartrees) between fragments A and B is the smallest in the geometry (STO-3G).

When Morokuma's energy partitions for both two geometries (STO-3G and 6-31G) of **1a** were performed at the same HF/6-31G level, we found that  $\Sigma\Delta E_{aq}$  values are  $-0.94030$  hartrees for the geometry (STO-3G) and  $-0.48538$  hartrees for one (6-31G), and their difference  $d(\Sigma\Delta E_{aq}) = \Sigma\Delta E_{aq}(6-31G) - \Sigma\Delta E_{aq}(\text{STO-3G}) = 0.45491$  hartrees. In a similar way,  $d(\Sigma\Delta E_{aq}^2) =$



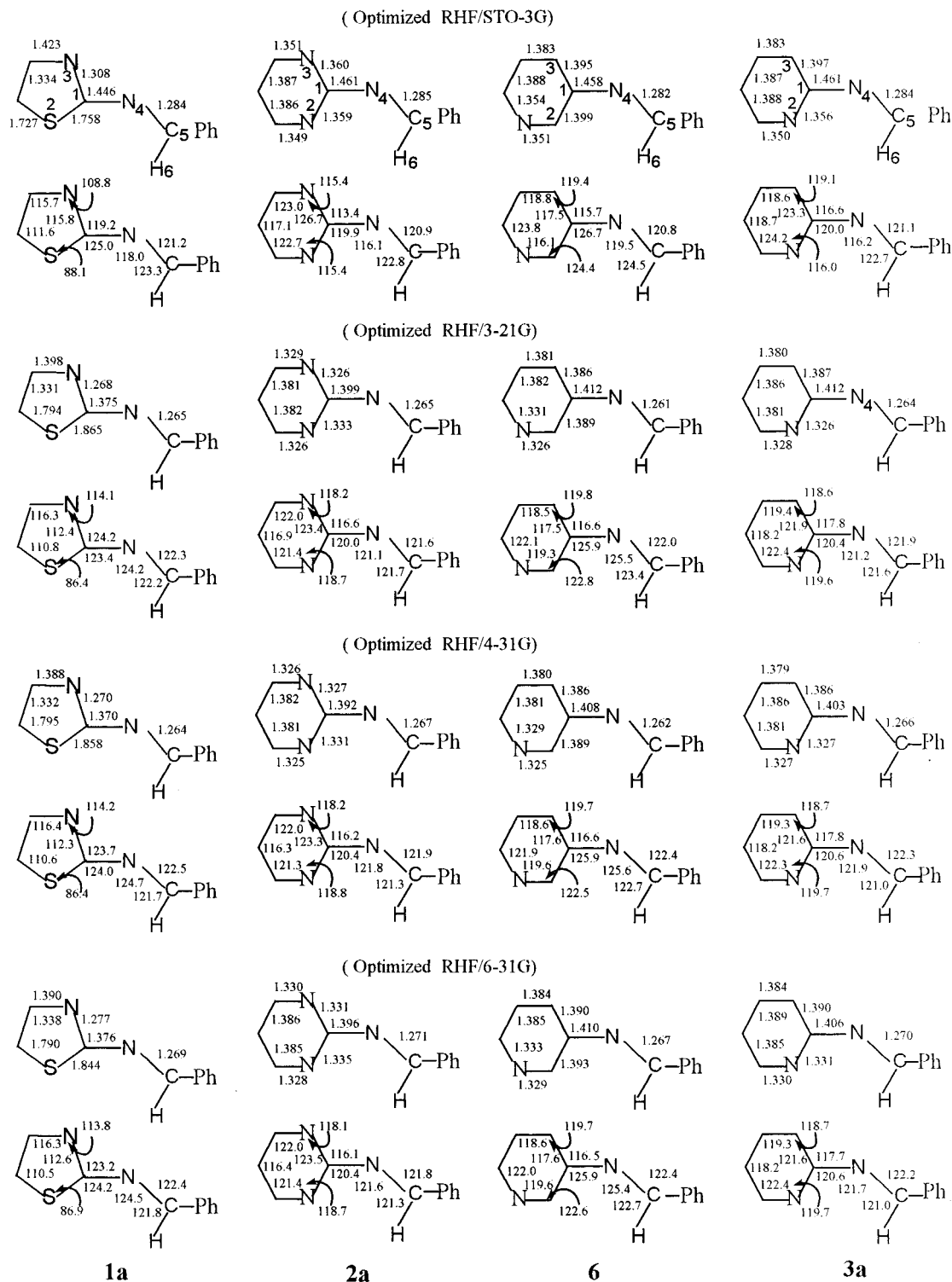


**Figure 8.** Planar optimized geometries obtained from the RHF/STO-3G, 3-21G, 4-31G, and 6-31G, respectively. The molecules **2a** and **3a** resulted from the replacement of a nitro group in **2** and **3** with a hydrogen atom.

$0.33772$  hartrees ( $d|\Sigma\Delta E_{aq}^2| = -0.33772$  hartrees),  $d(\Sigma\Delta E_{aq}^4) = 0.64403$  hartrees,  $d(V_{ab}) = 0.20974$  hartrees,  $d(A_{a,4}) = 0.86345$  hartrees ( $d|A_{a,4}| = -0.86345$  hartrees), and  $d(r_{14}) = -0.07$  Å. Similar to the  $d_{SH}$  distortion which was previously investigated by Shaik,<sup>23</sup> when  $r_{14}$  in the geometry (STO-3G) of **1a** is shortened from 1.446 to 1.416 Å while the length  $r_{57}$  of the bond C<sub>5</sub>-C<sub>7</sub> is lengthened from 1.4943 to 1.5283 Å, we get a planar  $d_{R14} = 1.416 - 1.446 = -0.03$  Å geometry where the contribution of the nuclear repulsion to the molecular energy of its original geometry (STO-3G) remains unchanged. On the

basis of the data in Tables 5–7, the stabilizing energy effects  $\Sigma\Delta E_{aq}$ ,  $\Sigma\Delta E_{aq}^2$ , and  $A_{a,4}$  are strengthened by  $-0.22741$ ,  $-0.45634$ , and  $-0.24396$  hartrees, respectively, if molecule **1a** was distorted from the geometry (STO-3G) to its  $d_{R14} = -0.03$  Å geometry (the  $d_{R14}$  torsion). Meanwhile,  $\Sigma\Delta E_{aq}^4$  (EX) and the molecule energy would be, respectively, increased by 0.23312 and 0.0023 hartrees. Additionally, the energy effect  $\Delta E_{bc}$ , associated with interaction between fragments B and C, is weakened by 0.08685 hartrees due to the  $d_{R14}$  torsion. The

**TABLE 5: Energy Effect  $\Sigma\Delta E_{aq}$  and Its CT and EX Components in the Ground State of Each of the Four Planar Geometries (STO-3G, 3-21G, 4-31G, and 6-31G), the Nuclear Repulsion  $V_{ab}$  between Fragments A and B, and Total Electronic Energy  $E_e$  (Energy Unit in hartrees)**

	STO-3G	3-21G	4-31G	6-31G
<b>1a</b>				
$\Sigma\Delta E_{aq}$	-5.80593 (-0.44604)	-3.04003 (-0.11308)	-1.33358 (0.13012)	-0.48538 (0.30712)
$V_{ab}$	108.21061	108.56686	108.59544	108.42035
$E_e$	-1642.50643	-1648.70135	-1652.36391	-1652.12174
$\Sigma\Delta E_{aq}^2$ (CT)	-6.32400 (-0.75904)	-8.07465 (-0.93485)	-6.35696 (-0.74186)	-5.45328 (-0.61350)
$\Sigma\Delta E_{aq}^4$ (EX)	0.55390 (0.34809)	4.73392 (0.88063)	5.40758 (0.93999)	5.78754 (0.98551)
<b>2a</b>				
$\Sigma\Delta E_{aq}$	-5.25930 (-0.40994)	-2.92358 (-0.18448)	-0.31990 (0.06363)	0.61061 (0.17082)
$V_{ab}$	100.4230	101.93979	102.02653	101.79994
$\Sigma\Delta E_{aq}^2$ (CT)	-5.93785 (-0.67777)	-7.47586 (-0.84279)	-5.30468 (-0.65032)	-4.32087 (-0.56765)
$\Sigma\Delta E_{aq}^4$ (EX)	0.72258 (0.31149)	4.14986 (0.72855)	5.24807 (0.79452)	5.61319 (0.81869)
<b>6</b>				
$\Sigma\Delta E_{aq}$	-5.29713 (-0.38234)	-2.87698 (-0.00418)	-2.78429 (0.27921)	-2.73241 (0.41872)
$V_{ab}$	97.46404	98.43510	98.60297	98.39205
$\Sigma\Delta E_{aq}^2$ (CT)	-6.09914 (-0.66423)	-8.09526 (-0.80285)	-8.11387 (-0.60543)	-7.86798 (-0.51213)
$\Sigma\Delta E_{aq}^4$ (EX)	0.83954 (0.31804)	4.59150 (0.82408)	5.30579 (0.91329)	5.50154 (0.95762)
<b>3a</b>				
$\Sigma\Delta E_{aq}$	-5.15184 (-0.38222)	-2.38450 (-0.09941)	-1.34048 (0.17039)	-0.97952 (0.28877)
$V_{ab}$	99.28844	100.41104	100.51951	100.30525
$\Sigma\Delta E_{aq}^2$ (CT)	-5.59352 (-0.66430)	-7.34891 (-0.81630)	-6.60561 (-0.62781)	-6.14682 (-0.54523)
$\Sigma\Delta E_{aq}^4$ (EX)	0.47631 (0.31746)	4.46705 (0.76461)	5.39960 (0.85121)	5.71409 (0.88612)

<sup>a</sup> Energy partition and geometry optimization at the same Gaussian basis level. The numbers in parentheses are the values of the  $\pi$  components.

difference in  $\Delta E_{bc}$  is rather smaller than in  $|\Sigma\Delta E_{aq}|$ . Therefore, the stabilizing energy effects prefer the optimized geometry (STO-3G) with the longer  $r_{14}$ .

Thus, it is really due to  $d(\text{EX})/d(r_{ab}) < 0.0$ ,  $d(\text{CT})/d(r_{ab}) < 0.0$  or their sum  $d(\text{EX})/d(r_{ab}) + d(\text{CT})/d(r_{ab}) < 0.0$  to reduce the bond length  $r_{14}$  as well as to shorten the average distance  $r_{ab} = K/V_{ab}$ , where  $K$  is a constant.

**3.4.4. Relationship between Bond Angle and Atomic Interaction Energy.** Figure 8 shows that in each of the molecules, the bond angle  $\angle C_5-N_4-C_1$  in the geometry (STO-3G) is the smallest of its related four geometries (STO-3G to 6-31G) and is getting larger as the Gaussian basis set increases from STO-3G to 4-31G. Equally, as shown by the data in Table 6, the ratio  $A_{a,5}/A_{a,b}$  for the geometry (STO-3G) is the greatest and decreases as the Gaussian basis increases. But it is not enough, only on the basis of such a relationship, to ascribe the smallest  $\angle C_5-N_4-C_1$  in the geometry (STO-3G) to the greatest  $A_{a,5}/A_{a,b}$  because its  $A_{a,5}$  is, after all, the least destabilizing of the four optimized geometries. The reducing of  $\angle C_5-N_4-C_1$  should increase the nuclear repulsion  $V_{ab}$ . On the basis of the geometric data in Figure 8, three possible ways to release the increase in  $V_{ab}$  are the following: lengthening the bond  $C_1-N_4$ ; increasing  $\Delta\alpha = \angle N_4-C_1-X_2 - \angle N_4-C_1-Y_3$  ( $X = C, N, S$ ;  $Y = C, N$ ); enlarging  $\angle H_6-C_5-N_4$ .

The theoretical bond angles in Figure 8 and the crystallographic data in Figure 9 show that the bond angle  $\angle N_4-C_1-X_2 > \angle N_4-C_1-Y_3$  is a general rule. In the crystal structure of molecule **2**, for example, the angle difference  $\Delta\alpha = \angle N_4-C_1-N_2 - \angle N_4-C_1-N_3$  is large up to  $10^\circ$ . In these two Figures, **1a** is an interesting molecule with the following distinguishing features: (i) all  $A_{k,4}$  ( $k \in$  fragment A and  $k \neq 1, 2, 3$ ) are much weaker than  $A_{3,4}$  and  $A_{2,4}$ ; (ii) at its geometry (STO-3G),  $A_{a,5} = 1.20854 > (A_{3,4} + A_{2,4}) = 1.01111$  hartrees, and  $V_{a,5} = 40.54419$  hartrees is the greatest of the four optimized geometries (STO-3G to 6-31G).

At the geometry (STO-3G) of **1a**,  $A_{3,4} = 0.60015 > A_{2,4} = 0.41096$  hartrees (Table 6), their difference  $dA_{3,2} = A_{3,4} - A_{2,4} = 0.18919$  hartrees. Correspondingly,  $\angle N_4-C_1-S_2 = 125.0^\circ$

$> \angle N_4-C_1-N_3 = 119.2^\circ$  and angle difference  $\Delta\alpha = 5.8^\circ$ . On the contrary, at its geometry (3-21G),  $A_{a,5} = 1.95021 < (A_{2,4} + A_{3,4}) = 2.56582$  hartrees,  $A_{3,4} = 1.05160 < A_{2,4} = 1.51422$  hartrees, and  $dA_{3,2} = -0.46262$  hartrees. Likewise,  $\angle N_4-C_1-S_2 = 123.4^\circ < \angle N_4-C_1-N_3 = 124.2^\circ$ , and  $\Delta\alpha = -0.8^\circ$ , which is only one exception to the general rule  $\angle N_4-C_1-X_2 > \angle N_4-C_1-Y_3$ . As far as the relationship between  $dA_{3,2}$  and  $\Delta\alpha$  as well as the ratio  $R_{5,4} = A_{a,5}/(A_{2,4} + A_{3,4})$  are concerned, the contrast between the two optimized geometries (STO-3G and 3-21G) of **1a** is so remarkable that it is reasonable to ascribe  $\Delta\alpha = -0.8^\circ$  in the optimized geometry (3-21G) to  $A_{2,4} > A_{3,4}$  because the nuclear repulsion  $V_{a,4}$  decreases as  $\angle N_4-C_1-S_2$  enlarges. As the Gaussian basis set is increased from 3-21G to 6-31G,  $A_{2,4} > A_{3,4}$  is kept, but  $dA_{3,2}$  monotonically increases from  $-0.46262$  (3-21G) through  $-0.19239$  (4-31G) to  $-0.05017$  hartrees (6-31G), and the ratio  $R_{5,4}$  decreases from 0.75 (3-21G) through 0.5 (4-31G) to 0.42 (6-31G). In the meanwhile,  $\Delta\alpha$  increases in the following sequence:  $-0.8^\circ$  (3-21G)  $< 0.3^\circ$  (4-31G)  $< 1.0^\circ$  (6-31G). The  $d_{\Delta\alpha}$  distortion analysis is necessary in order to reveal the driving forces for enlarging  $\Delta\alpha$ .

As shown by the  $d_{\Delta\alpha}$  distortion where  $d_{\Delta\alpha} = \Delta\alpha(d_{\Delta\alpha}) - \Delta\alpha(d_{\Delta\alpha} = 0)$ , the increase in  $\Delta\alpha$  is also an effective way to weaken the stabilizing interaction energies, such as  $\Sigma\Delta E_{aq}$ , CT,  $A_{1,4}$ , and  $A_{a,4}$ , as well as to strengthen the destabilizing EX energy besides its releasing the nuclear repulsion  $V_{a,4}$  (Table 7). At the  $d_{\Delta\alpha} = 0$  geometry, i.e., the optimized geometry (STO-3G) of **1a**, for example, its  $\Sigma\Delta E_{aq}$  ( $-5.80593$  hartrees),  $\Sigma\Delta E_{aq}^2$  ( $-6.32400$  hartrees), and  $A_{1,4}$  ( $-8.10377$  hartrees) are least stabilizing and become more stabilizing while its  $\Sigma\Delta E_{aq}^4$  is getting less destabilizing as its  $\Delta\alpha$  decreases from  $5.8422^\circ$  in the  $d_{\Delta\alpha} = 0$  geometry to  $-0.5578^\circ$  in the  $d_{\Delta\alpha} = -6.4^\circ$  geometry. Similar to the  $d_{R14}$  distortion, in the case of molecule **1a**, the  $d_{\Delta\alpha}$  geometry arises from variations in the four bond angles,  $\angle N_4-C_1-S_2$ ,  $\angle N_4-C_1-N_3$ ,  $\angle C_5-N_4-C_1$  and  $\angle H_6-C_5-N_4$ , within the constraint that the contribution of the nuclear repulsion to the total molecular energy of the optimized geometry (STO-3G) remains constant. The  $d_{\Delta\alpha}$  distortion deforms fragments A and B + C, and total electronic energy

**TABLE 6: Various Atomic Interaction Energies between Fragments A and B + C in the Ground State of Each of Four Planar Geometries (STO-3G, 3-21G, 4-31G, and 6-31G), and the Related Nuclear Repulsion Energies (Energy Unit in hartrees)<sup>a</sup>**

	STO-3G	3-21G	4-31G	6-31G
<b>1a</b>				
$A_{ab}$	2.33841 (0.09458)	4.40656 (0.40722)	5.06467 (0.50977)	5.15338 (0.60599)
$A_{1,4}$	-8.10377 (-0.54051)	-7.32631 (-0.52197)	-6.23075 (-0.38131)	-5.42370 (-0.29978)
$A_{2,4}$	0.41096 (0.01125)	1.51422 (0.06956)	1.87728 (0.08668)	1.94485 (0.11765)
$A_{3,4}$	0.60015 (0.02713)	1.05160 (0.13407)	1.68489 (0.22304)	1.89468 (0.24401)
$A_{a,4}$	-7.13154 (-0.50196)	-4.83317 (-0.31960)	-2.81511 (-0.07570)	-1.77092 (0.05522)
$V_{a,4}$	60.62813	61.56992	61.72233	61.62732
$A_{a,5}$	1.20854 (0.05603)	1.95021 (0.20485)	1.71227 (0.20416)	1.62037 (0.25098)
$V_{a,5}$	40.54419	40.12856	40.03032	39.96708
$A_{a,6}$	0.15764 (0.00000)	-0.03679 (0.00000)	-0.06324 (0.00000)	-0.11987 (0.00000)
$V_{a,6}$	7.03829	6.86838	6.84288	6.82595
<b>2a</b>				
$A_{ab}$	2.60144 (0.08777)	5.36486 (0.34293)	7.37072 (0.51140)	7.95140 (0.57577)
$A_{1,4}$	-7.81944 (-0.49767)	-8.15071 (-0.53024)	-7.53156 (0.06789)	-7.15791 (-0.40772)
$A_{a,4}$	-6.57254 (-0.44903)	-4.72196 (-0.31828)	-1.77618 (-0.09445)	-0.91652 (-0.01442)
$V_{a,4}$	56.85545	58.37542	58.55867	58.41279
$A_{a,5}$	1.18476 (0.03912)	2.14561 (0.13098)	1.78697 (0.15556)	1.87650 (0.18248)
$V_{a,5}$	37.24388	37.31265	37.23863	37.16656
$A_{a,6}$	0.16978 (0.00000)	-0.20905 (0.00000)	-0.17163 (0.00000)	-0.16649 (0.00000)
$V_{a,6}$	6.32370	6.25172	6.22923	6.22059
<b>6</b>				
$A_{ab}$	2.45807 (0.10292)	4.23560 (0.45269)	4.21665 (0.54997)	4.23159 (0.62684)
$A_{1,4}$	-7.71759 (-0.48512)	-7.03883 (-0.45806)	-6.91770 (-0.27110)	-6.88078 (-0.20791)
$A_{a,4}$	-6.53913 (-0.44227)	-4.48661 (-0.24715)	-4.25800 (0.00199)	-4.16612 (0.09922)
$V_{a,4}$	55.54212	56.74002	56.85788	56.72767
$A_{a,5}$	1.09003 (0.06007)	1.78155 (0.24178)	1.68129 (0.27688)	1.66402 (0.31970)
$V_{a,5}$	35.94582	35.83384	35.86178	35.78955
$A_{a,6}$	0.18957 (0.00000)	-0.09817 (0.00000)	-0.12433 (0.00000)	-0.14709 (0.00000)
$V_{a,6}$	5.97610	5.86124	5.88331	5.87483
<b>3a</b>				
$A_{ab}$	2.61274 (0.09948)	5.12045 (0.39381)	5.99031 (0.53786)	6.25271 (0.61047)
$A_{1,4}$	-7.72374 (-0.48164)	-7.37644 (-0.49551)	-7.20727 (-0.36904)	-7.11364 (-0.32316)
$A_{a,4}$	-6.44955 (-0.43485)	-4.10311 (-0.27764)	-2.66349 (-0.04860)	-2.25004 (0.03503)
$V_{a,4}$	56.12162	57.38780	57.55791	57.43335
$A_{a,5}$	1.17296 (0.05268)	2.07943 (0.17594)	1.68479 (0.21742)	1.64655 (0.25228)
$V_{a,5}$	36.89239	36.84431	36.79211	36.71384
$A_{a,6}$	0.16559 (0.00000)	-0.23231 (0.00000)	-0.23825 (0.00000)	-0.25744 (0.00000)
$V_{a,6}$	6.27444	6.17894	6.16948	6.15807

<sup>a</sup> Energy partition and geometry optimization at the same Gaussian basis level. The numbers in parentheses are the values of the corresponding  $\pi$  components.

**TABLE 7: Energy Components in the Optimized Geometry (STO-3G) of 1a and Their Changes with the  $d_{R14}$  and  $d_{\Delta\alpha}$  Distortion (Energy Unit in hartrees)**

	$d_{R14}$ torsion		$d_{\Delta\alpha}$ torsion	
	$d_{R14} = -0.03$	$d_{R14} = 0.0^a$ , $d_{\Delta\alpha} = 0.0^a$	$d_{\Delta\alpha} = -3.0$	$d_{\Delta\alpha} = -6.4$
$r_{14}$ (Å)	1.41603	1.44603	1.44603	1.44603
$r_{57}$ (Å)	1.52835	1.49430	1.49430	1.49430
$\angle N_4-C_1-S_2$	125.04200	125.04200	123.54200	121.84200
$\angle N_4-C_1-N_3$	119.19980	119.19980	120.69980	122.39980
$\angle C_5-N_4-C_1$	118.00800	118.00800	119.07841	120.35948
$\angle H_6-C_5-N_4$	123.34700	123.34700	123.80575	124.35478
$\Sigma\Delta E_{aq}$	-6.03341	-5.80593	-5.87403	-5.94608
$V_{ab}$	109.36925	108.21061		
$\Sigma\Delta E_{aq}^2$ (CT)	-6.78034	-6.32400	-6.38721	-6.45603
$\Sigma\Delta E_{aq}^4$ (EX)	0.78702	0.55390	0.54902	0.54577
$A_{1,4}$	-8.40783	-8.10377	-8.12489	-8.14971
$A_{a,4}$	-7.37550	-7.13154	-7.16256	-7.19282
$V_{a,4}$	61.49130	60.62813	60.67824	60.74817
$E_e$	-1642.50413	-1642.50643	-1642.50619	-1642.50534

<sup>a</sup> The optimized geometry (STO-3G).  $d_{\Delta\alpha} = \Delta\alpha(d_{\Delta\alpha}) - \Delta\alpha(0.0)$ ,  $\Delta\alpha = \angle N_4-C_1-S_2 - \angle N_4-C_1-N_3$ ;  $d_{R14} = r_{14}(d_{R14}) - r_{14}(0.0)$ .

of fragment molecule FM-P (P = A, B + C), in itself, should be different from one  $d_{\Delta\alpha}$  geometry to another one according to Figure 2. However, the full RHF computations for various isolated fragment molecule FM-P show that the difference in total electronic energy of the fragment P between two  $d_{\Delta\alpha}$  torsion geometries is much smaller than the differences in the

energy effects, such as  $\Sigma\Delta E_{aq}$ ,  $\Sigma\Delta E_{aq}^2$  and  $\Sigma\Delta E_{aq}^4$ , etc., associated with the inter- and intrafragment interactions.

**3.4.5. Relationship between the Nuclear Repulsion and Interaction Energy Effect.** As mentioned previously, when the nuclear repulsion energies  $V_{ab}$  is used to measure the average distance  $r_{ab}$ , we can find the following general tendencies: A larger  $V_{ab}$  generally corresponds to a less stabilizing or a greater destabilizing energy effects. In three optimized geometries (STO-3G to 4-31G) of molecule **2a**, for example, the nuclear repulsion  $V_{ab}$  increases in the sequence: 100.4230 (STO-3G) < 101.93979 (3-21G) < 102.02653 hartrees (4-31G), and the corresponding  $\Sigma\Delta E_{aq}$ ,  $R_{XC}$ , and the length  $r_{1,4}$  change in the following sequences:  $\Sigma\Delta E_{aq}$ , -5.25930 (STO-3G) < -2.92358 (3-21G) < -0.31990 hartrees (4-31G);  $R_{XC}$ , 0.078 (STO-3G) < 0.515 (3-21G) < 0.96;  $r_{1,4}$ , 1.461 (STO-3G) > 1.399 (3-21G) > 1.392 Å (4-31G). It confirms once more that the local destabilizing (stabilizing) interaction is practically attractive (repulsive).

## Summary

The distinction between the exchange and CT delocalization makes it possible to reevaluate the conventional explanation of organic chemistry.<sup>24</sup> The local destabilizing EX interaction between fragments is basically stabilization as far as its effect on whole electronic state is considered. Correspondingly, the

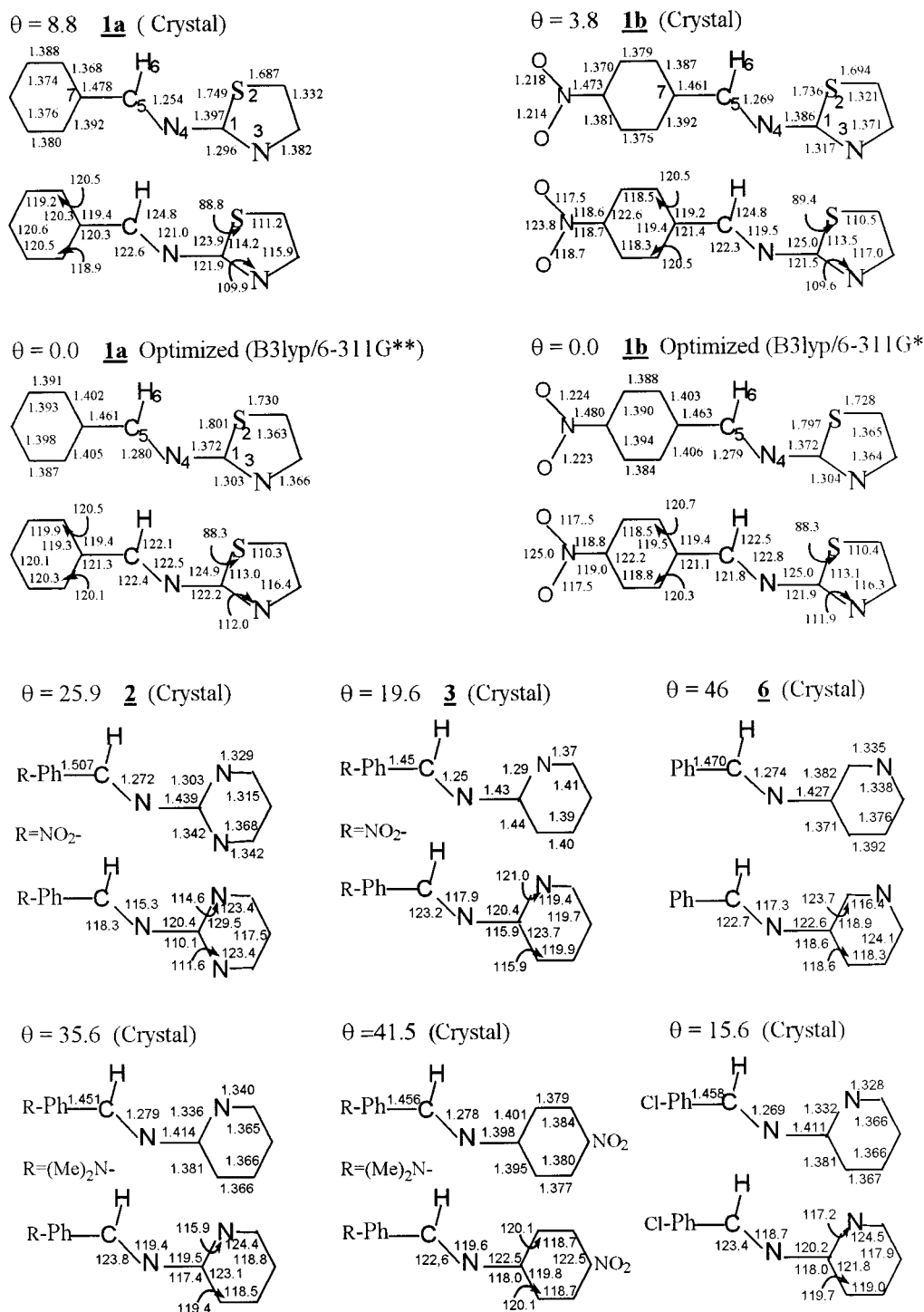


**Figure 9.** Crystal structures of typical stilbene-like species and the preferential geometries of **1a** and **1b**.

stabilizing CT interaction is practically destabilization. Thus, at the planar geometry of stilbene-like species, it is  $d(\text{CT})/d(r_{ab}) < 0.0$ ,  $d(\text{EX})/d(r_{ab}) < 0.0$ , or the sum  $d(\text{CT})/d(r_{ab}) + d(\text{EX})/d(r_{ab}) < 0.0$  to reduce the length of the bond  $\text{C}_1\text{--N}_4$  as well as to shorten the distance between fragments. A stilbene-like species has to distort itself away from its planar geometry in order to maintain the lowest total electronic energy as far as possible when the attractive force  $d(E_e)/d(r_{ab}) > 0.0$ , arising from  $d(\text{CT})/d(r_{ab}) + d(\text{EX})/d(r_{ab}) < 0.0$ , is not large enough to balance the resistance force  $d(V_{ab})/d(r_{ab}) < 0.0$ . Various total energy effects  $\Delta E^V$ ,  $\Delta E^G$ , and  $\Delta E^{(\sigma)}$  associated with the  $\pi\text{--}\pi$ ,  $\pi\text{--}\sigma$ , and nonbonded  $\sigma\text{--}\sigma$  interactions at the RHF/STO-3G level, together with their changes with the torsional angle  $\theta$ ,

are summarized in Figure 10. As we have concluded, these three types of electron delocalization are always destabilization. The  $\sigma$  electron plays an important role in determining geometry of stilbene-like species, and the nonbonded  $\sigma\text{--}\sigma$  interaction is the greatest driving force for distorting molecule away from its geometry with  $\theta = 0^\circ$ . Contrary to the classical viewpoint, the  $\pi\text{--}\pi$  interaction is also a driving force, but it has only a slight effect on the molecular geometry.

At a rotational geometry with  $\theta = 52^\circ$  (Figure 10),  $d(\Delta E(\theta))/d|\theta| = 0$ , a compromise between the nonbonded  $\sigma\text{--}\sigma$  and the  $\pi\text{--}\sigma$  interactions, is a common feature of the stilbene-like species such as **1a**, **1b**, and **6**. Particularly, the driving force,  $d(\Delta E^V(\theta))/d|\theta| + d(\Delta E^{(\sigma)}(\theta))/d|\theta| + d(\Delta E^G(\theta))/d|\theta|$  in Figure



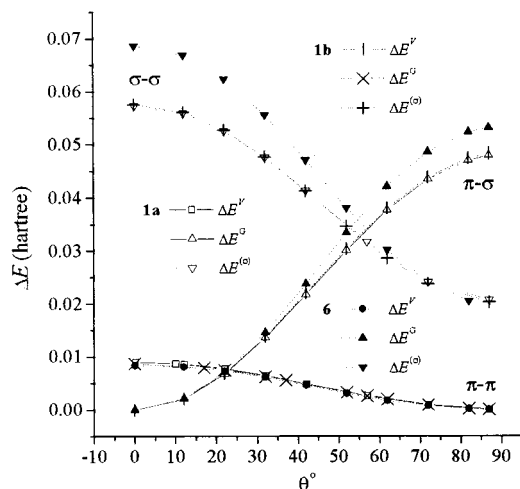


**Figure 10.** Energy effects  $\Delta E^V$ ,  $\Delta E^G$ , and  $\Delta E^{(\sigma)}$ , respectively, associated with the  $\pi$ - $\pi$ ,  $\pi$ - $\sigma$ , and the nonbonded  $\sigma$ - $\sigma$  interactions at the STO-3G level and their changes with the torsional angle  $\theta$ .

10, is approximately in accord with that  $d(\Delta E_c(\theta))/d|\theta| = d(E_c(\theta))/d|\theta|$  described in Figures 1 and 4. The conclusions derived from the Morokuma's energy partitioning analysis should be reasonable because  $d(\Delta E_c(\theta))/d|\theta|$  described in Figures 1 and 4 were obtained from the well-known methods such as HF, DFT, MP2, and AM1 in the standard Gaussian 98 program.

## Experimental Section

**General Methods.** All starting materials were obtained commercially as reagent-grade. Melting points were determined on a Nagoya apparatus and are uncollected. Crystal structures of molecules were determined by Nicolet R3WE X-ray diffractometer.

**N-phenylmethylene-2-thiazoleamine (1a)** was obtained as a bright yellow crystal from benzaldehyde and 2-aminothiazole.<sup>25</sup> mp 44.5–45 °C. <sup>1</sup>H NMR(CDCl<sub>3</sub>): 9.04 (s, 1H), 8.00–7.96 (2d, 2H), 7.68 (d, 1H), 7.51 (m, 3H), 7.31 (d, 1H). Crystal data: wt. 188.24. Orthorhombic,  $a = 21.652$  (4),  $b = 29.146$  (6),  $c = 5.927$  (2) Å, cell volume = 3740 Å<sup>3</sup>,  $D_{\text{cal}} = 1.337$  mg/m<sup>3</sup>. Mo K $\alpha$  radiation  $\lambda = 0.71073$  Å. Space group *Fdd2*.

**N-(4-nitrophenyl)methylene-2-thiazoleamine (1b)** was obtained as a yellow crystal from 4-nitrobenzaldehyde and 2-aminothiazole using the same procedure as that for preparing **1a**. mp 184–185 °C. <sup>1</sup>H NMR (CDCl<sub>3</sub>): 9.18 (s, 1H), 7.74–7.35 (d, 2H). Crystal data: wt. 233.25. Triclinic,  $a = 8.427$  (2),  $b = 9.679$  (2),  $c = 6.1930$  (10) Å,  $\alpha = 93.83^\circ$  (3°),  $\beta = 90.09^\circ$  (3°),  $\gamma = 95.44^\circ$  (3°), cell volume = 501.72 (18) Å<sup>3</sup>,  $D_{\text{cal}} = 1.544$  mg/m<sup>3</sup>. Mo K $\alpha$  radiation  $\lambda = 0.71073$  Å. Space group *P1̄*.

**N-phenylmethylene-1-naphthylamine (4)** was obtained as a bright yellow crystal from 1-aminonaphthalene and benzaldehyde.<sup>26</sup> mp 76.1 °C (lit.,<sup>27</sup> 73–75 °C). <sup>1</sup>H NMR(DMSO-*d*<sub>6</sub>): 8.50 (s, 1H), 7.01 (s, 1H), 7.2–8.0 (m, 10H), 8.29 (s, 1H). Crystal data: wt. 231.28. Orthorhombic,  $a = 22.967$  (5),  $b = 14.924$  (3),  $c = 7.263$  (10) Å, cell volume = 2489.5 (8) Å<sup>3</sup>,  $D_{\text{cal}} = 1.234$  mg/m<sup>3</sup>. Mo K $\alpha$  radiation  $\lambda = 0.71073$  Å. Space group *Pbca*.

**Acknowledgment.** This work is supported by the National Natural Science Foundation of China (Grants 29872042, 20072041, and 20032010).

## References and Notes

- (1) (a) Streitwieser, A.; Heathcock, C. H. *Introduction to Organic Chemistry*; Macmillan Publishing Company: New York, 1985. (b) Neckers, D.; Doyle, M. P. *Organic Chemistry*; John Wiley & Sons: New York, 1977. (c) March, J. *Advanced Organic Chemistry*; John Wiley & Sons: New York, 1992.
- (2) Gould, E. S. *Mechanism and Structure in Organic Chemistry*; Henry Holt and Company: New York, 1960.
- (3) (a) Yu, Z. H.; Li, L. T.; Fu, W.; Li, L. P. *J. Phys. Chem. A* **1998**, *102*, 2016. (b) Yu, Z. H.; Xuan, Z. Q.; Wang, T. X.; Yu, H. M. *J. Phys. Chem. A* **2000**, *104*, 1736. (c) Yu, Z. H.; Xuan, Z. Q. *THEOCHEM* **1999**, *488*, 101. (d) Yu, Z. H. *Comput. Chem.* **1994**, *18*, 95. (e) Yu, Z. H. *Int. J. Quantum Chem.* **1995**, *55*, 485.
- (4) (a) Zamir, S.; Bernstein, J.; Loffe, A.; Brunovll, J.; Kolonits, M.; Hargittai, I. *J. Chem. Soc., Perkin Trans. 2*, **1994**, 895, and refs cited therein. (b) Curtis, R. D.; Penner, G. H.; Power, W.; Wasylshen, R. E. *J. Phys. Chem.* **1990**, *94*, 400.
- (5) (a) Skrabal, P.; Steiger, J. *Helv. Chim. Acta.* **1975**, *58*, 800. (b) Bernstein, J.; Anderson, T. E.; Eckhardt, C. J. *J. Am. Chem. Soc.* **1979**, *101*, 541. (c) Patnaik, L. N. and Das, S. *Int. J. Quantum Chem.* **1985**, *27*, 135. (d) Akaba, R.; Tokumaru, K.; Kobayashi, T. *Bull. Chem. Soc. Jpn.* **1980**, *53*, 1993. (e) Akaba, R.; Sakuragi, H.; Tokumaru, K. *Bull. Chem. Soc. Jpn.* **1985**, *58*, 1186.
- (6) (a) Burgi, H. B.; Dunitz, J. D. *Helv. Chim. Acta* **1971**, *54*, 1255. (b) Choi, C. H.; Kertesz, M. *J. Phys. Chem. A* **1997**, *101*, 3823. (c) Kuze, N.; Ebizuka, M.; Fujiwara, H.; Takeuchi, H.; Egawa, T.; Konaka, S. *J. Phys. Chem. A* **1998**, *102*, 2080.
- (7) (a) Müller, M.; Hohlneicher, G. *J. Am. Chem. Soc.* **1990**, *112*, 1273. (b) Kendrick, J. *J. Chem. Soc., Faraday Trans.* **1990**, *86*, 3995.
- (8) (a) Traetteberg, M.; Hilmlo, I.; Hagen, K. *J. Mol. Struct.* **1977**, *39*, 231. (b) Traetteberg, M. Frantsen, E. B.; Mijlhoff, F. C.; Hoekstra, A. *J. Mol. Struct.* **1975**, *26*, 57.
- (9) Nakai, H.; Shiro, M.; Ezumi, K.; Sakata, S.; Kubota, T. *Acta Crystallogr.* **1976**, *B32*, 1827.
- (10) Wiebcke, M.; Mootz, D. *Acta Crystallogr.* **1982**, *B38*, 2008.
- (11) Epiotis, N. D.; Cherry, W. R.; Shaik, S.; Yates, R.; Bernardi, F. *Top. Curr. Chem.* **1977**, *70*.
- (12) (a) Yu, Z. H.; Xuan, Z. Q. *Chem. J. Chin. Univ.* **2000**, *21*, 421. (b) Yu, Z. H.; Peng, X. Q.; Xuan, Z. Q. *Chin. J. Org. Chem.* **2000**, *20*, 882.
- (13) Kitaura, K.; Morokuma, K. *Int. J. Quantum Chem.* **1976**, *10*, 325.
- (14) Dewar, M. J. S.; Dougherty, R. C. *The PMO Theory of Organic Chemistry*; Plenum Press: New York and London, 1975.
- (15) Kollmar, H. *J. Am. Chem. Soc.* **1979**, *101*, 4832.
- (16) Glendenning, E. D.; Faust, R.; Streitwieser, K. Vollhardt, P. C. and Weinhold, F. *J. Am. Chem. Soc.* **1993**, *115*, 10952.
- (17) (a) Mulliken, R. S.; Parr, R. G. *J. Chem. Phys.* **1951**, *19*, 1271. (b) Bernardi, F.; Bottoai, N. D.; Epiotis, N. D.; G, M. *J. Am. Chem. Soc.* **1978**, *100*, 6018.
- (18) (a) Salem, L. *J. Am. Chem. Soc.* **1968**, *90*, 543. (b) Whangbo, M. H.; Schlegel, H. B.; Wolfe, S. *J. Am. Chem. Soc.* **1977**, *99*, 1296. (c) Kraut, A. *Rev. Biochem.* **1977**, *46*, 331. (d) Bingham, R. C.; Dewar, M. J. S.; Lo, D. H. *J. Am. Chem. Soc.* **1975**, *97*, 1285. (e) Csizmadia, I. G. *Molecular Structure and Conformation*; Elsevier: Amsterdam, 1982.
- (19) Libit, L.; Hoffmann, R. *J. Am. Chem. Soc.* **1974**, *96*, 1370.
- (20) Csizmadia, I. G. *Theory and Practice of MO Calculation on Organic Molecules*; Elsevier: Amsterdam, 1976.
- (21) Bader, P. F. W.; Streitwieser, A.; Neuhaus, A.; Laidig, K. E.; Speers, P. *J. Am. Chem. Soc.* **1996**, *118*, 4959.
- (22) Reed, A.; Curtiss, L. A.; Weinhold, F. *Chem. Rev.* **1988**, *88*, 899.
- (23) Shaik, S. S.; Hiberty, P. C.; Lefour, J. M.; Ohanessian, G. *J. Am. Chem. Soc.* **1987**, *109*, 363.
- (24) Epiotis, N. D. *Deciphering the Chemical Code*; VCH Publishers: New York, 1996.
- (25) Singh, N.; Sethi, P. S. *J. Indian Chem. Soc.* **1975**, *52*, 1079.
- (26) Britta, M. D.; Otto, D. *Acta Chem. Scand.* **1969**, *23*, 1503.
- (27) Crossley, M. L.; Dreisbach, P. F.; Hofmann, C. M.; Parker, R. P. *J. Am. Chem. Soc.* **1952**, *74*, 573.